JACS
JOURNAL OF THE AMERICAN CHEMICAL SOCIETY

ARTICLE

pubs.acs.org/JACS

Proton Transfer Drives Protein Radical Formation in *Helicobacter pylori* Catalase but Not in *Penicillium vitale* Catalase

M. Alfonso-Prieto,[†,‡] H. Oberhofer,[§] M. L. Klein,[‡] C. Rovira,[*,†,∥,⊥] and J. Blumberger[*,#]

[†]Computer Simulation & Modeling Laboratory, Parc Científic de Barcelona, Baldiri Reixac 4, 08028 Barcelona, Spain

[‡]Institute for Computational Molecular Science, Temple University, 1900 North 12th Street, Philadelphia, Pennsylvania 19122, United States

[§]Department of Chemistry, University of Cambridge, Lensfield Road, Cambridge CB2 1EW, United Kingdom

[∥]Institut de Química Teòrica i Computacional (IQTCUB), Universitat de Barcelona, 08028 Barcelona, Spain

[⊥]Institució Catalana de Recerca i Estudis Avançats (ICREA), 08010 Barcelona, Spain

[#]Department of Physics and Astronomy, University College London, London WC1E 6BT, United Kingdom

Supporting Information

ABSTRACT: Heme catalases prevent cells from oxidative damage by decomposing hydrogen peroxide into water and molecular oxygen. Here we investigate the factors that give rise to an undesirable side reaction competing with normal catalase activity, the migration of a radical from the heme active site to the protein in the principal reaction intermediate compound I (Cpd I). Recently, it has been proposed that this electron transfer reaction takes place in Cpd I of *Helicobacter pylori* catalase (HPC), but not in Cpd I of *Penicillium vitale* catalase (PVC), where the oxidation equivalent remains located on the heme active site. Unraveling the factors determining the different radical locations could help engineer enzymes with enhanced catalase activity for detection or removal of hydrogen peroxide. Using quantum mechanics/molecular mechanics metadynamics simulations, we show that radical migration in HPC is facilitated by the large driving force (−0.65 eV) of the subsequent proton transfer from a histidine residue to the ferryl oxygen atom of reduced Cpd I. The corresponding free energy in PVC is significantly smaller (−0.19 eV) and, as we argue, not sufficiently high to support radical migration. Our results suggest that the energetics of oxoferryl protonation is a key factor regulating radical migration in catalases and possibly also in hydroperoxidases.

1. INTRODUCTION

Heme catalases are present in almost all aerobically respiring organisms. They play an important role in defending cells against oxidative damage by degrading hydrogen peroxide to water and oxygen ($2H_2O_2 \rightarrow 2H_2O + O_2$).[1] Catalases carry out this reaction in a remarkably efficient manner, which is why they have also found applications in the food and textile industries for detection and removal of hydrogen peroxide.[1b] However, under certain conditions the efficiency of the catalase reaction can decrease due to competition with undesirable side reactions that increase the risk of oxidative damage of the cell. Altered catalase activity levels have been implicated as an important factor in inflammation,[2] mutagenesis,[3] prevention of apoptosis,[4] and stimulation of a wide spectrum of tumors.[5] Here we aim to understand the factors that lead to a particular side reaction competing with the main catalase activity, the oxidation of the protein by its own heme cofactor (reaction 4).

The catalase reaction takes place in two steps. First, the resting state of the enzyme reacts with one molecule of hydrogen peroxide to form water and an oxoferryl porphyrin cation radical ($Por^{\bullet+}—Fe^{IV}=O$), termed compound I (Cpd I):

$$\text{Enz}\ (\text{Por} - \text{Fe}^{\text{III}}) + H_2O_2 \rightarrow \text{Cpd I}\ (\text{Por}^{\bullet+}—\text{Fe}^{\text{IV}}=\text{O}) + H_2O \quad (1)$$

The latter is a highly oxidizing species that converts a second molecule of hydrogen peroxide into molecular oxygen, thereby closing the catalytic cycle:

$$\text{Cpd I}\ (\text{Por}^{\bullet+}—\text{Fe}^{\text{IV}}=\text{O}) + H_2O_2 \rightarrow \text{Enz}\ (\text{Por} - \text{Fe}^{\text{III}}) + H_2O + O_2 \quad (2)$$

Reactions 1 and 2 constitute the main activity of catalases. However, at low H_2O_2 concentrations and in the presence of certain organic substrates (AH, e.g., phenols), Cpd I can also undergo a one-electron reduction to form another intermediate, termed compound II (Cpd II):

$$\text{Cpd I}\ (\text{Por}^{\bullet+}—\text{Fe}^{\text{IV}}=\text{O}) + \text{AH} \rightarrow \text{Cpd II}\ (\text{Por} - \text{Fe}^{\text{IV}} - \text{OH}) + \text{A}^{\bullet} \quad (3)$$

Received: May 20, 2010
Published: March 07, 2011

dx.doi.org/10.1021/ja1110706 | *J. Am. Chem. Soc.* 2011, 133, 4285–4298

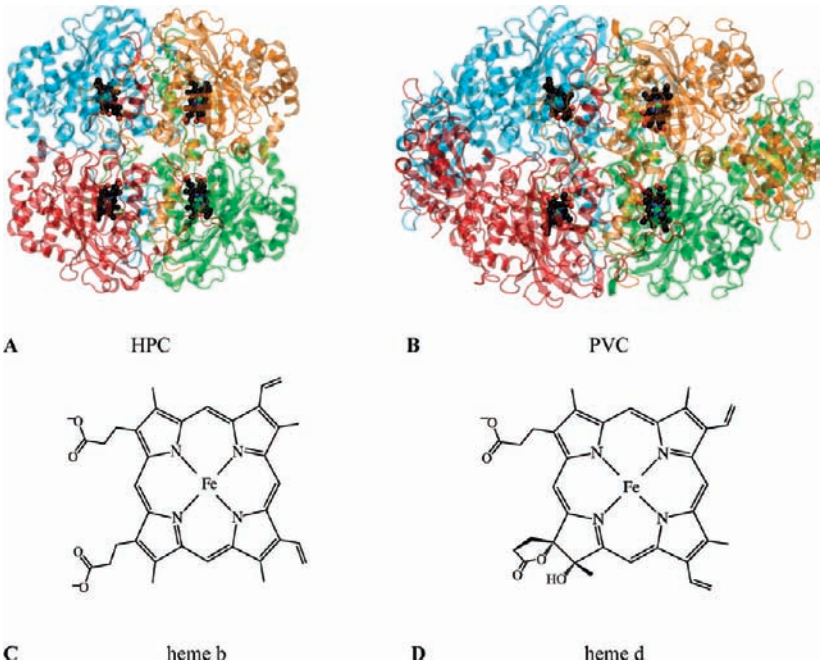

Figure 1. Structures of HPC (A) and PVC (B). The protein is shown in cartoon respresentation with the four subunits colored in blue, red, yellow, and green, respectively, and the heme groups are shown in CPK representation. The molecular structures of heme b (C) and heme d (D) prosthetic groups of HPC and PVC, respectively, are also displayed.

Interestingly, in the absence of AH, an endogenous protein residue (aa), usually Tyr or Trp, can also reduce Cpd I:

$$\text{Cpd I } (\text{Por}^{\bullet+}\text{—Fe}^{\text{IV}}\text{=O} + \text{H}^+ + \text{aa}) \rightarrow \text{Cpd I*}$$
$$(\text{Por} - \text{Fe}^{\text{IV}} - \text{OH} + \text{aa}^{\bullet(+)}) \qquad (4)$$

The intramolecular electron transfer (ET) reaction 4 is often referred to as "migration of the porphyrin radical into the protein", and this process is normally concomitant with protonation of the oxoferryl bond.[6] In fact, radical migration in catalases[6a] and other heme proteins[7] correlates with the observation of lengthening of the Fe−O distance (from 1.6−1.7 to 1.8−1.9 Å), indicative of a change from oxoferryl, Fe=O, to hydroxoferryl, Fe−OH. The most likely proton donor was identified in ref 6a to be the distal His.

Whereas for some heme proteins (e.g., in cytochrome *c* peroxidases,[7a] catalase peroxidases,[7b] or lactoperoxidase[8]), formation of a protein radical (i.e., Cpd I*) is necessary for mediating the electron transfer between the heme and the substrate, radical migration in catalases[9] and P450[10] is considered an undesirable side reaction that competes with the main activity of the enzyme. Nevertheless, reaction 4 has been suggested to be the main catalase mechanism for Cpd I reduction in cells with low H_2O_2 concentrations.[11] Under these conditions, Cpd I reduction by hydrogen peroxide is slow and the alternative reduction by protein residues could avoid a prolonged or frustated Cpd I state that would result in an irreversible inactivation of the enzyme. In peroxidases, it has been proposed that Cpd I* is an alternative reactive intermediate in the oxidation of bulky substrates that cannot access the heme active site.[12] Therefore, understanding the factors leading to radical migration could help to engineer new catalytically competent protein radical sites for the oxidation of substrates that cannot be oxidized at the heme active site.[13]

The factors that govern radical migration in specific heme enzyme families such as catalases are poorly understood. Recently, UV−vis spectroscopy and X-ray crystallography have been used to study the Cpd I intermediates of *Helicobacter pylori* catalase (HPC; Figure 1A) and *Penicillium vitale* catalase (PVC; Figure 1B). HPC is a bacterial enzyme that can be used to study oxidative stress because it is similar to mammalian catalases and overexpression and mutagenesis are easier than for the eukaryotic enzymes,[11b] whereas PVC is used to remove the excess hydrogen peroxide in food products.[1b] The results obtained suggest that HPC forms a protein radical, in contrast to PVC, where the radical remains on the heme.[6a] The different types of intermediates that are formed (Cpd I* for HPC and Cpd I for PVC) could be related to the type of heme present, heme b in HPC and heme d in PVC (see panels C and D, respectively, of Figure 1). However, it is known that heme b catalases different from HPC do form canonical Cpd I.[14] Therefore, factors other than the type of heme are likely to influence radical migration in catalases.

Knowledge of the reduction potentials of the catalase Cpd I intermediates of HPC and PVC would help to clarify this issue. Unfortunately, these are not available due to the short lifetime of this redox intermediate. Using quantum mechanics/molecular mechanics (QM/MM) molecular dynamics (MD) simulations, we show herein that the difference in free energy for pure one-electron reduction of Cpd I ("pure" means without coupled proton transfer (PT)) is indeed very small and unlikely to be the reason for the different redox behaviors of HPC and PVC. Our simulations give evidence that it is the subsequent PT step from a neighboring histidine residue to the ferryl oxygen that provides the major driving force for radical migration. The thermodynamic picture obtained for radical migration in the two catalases may apply to other heme proteins forming Cpd I*.

This paper is organized as follows. In section 2 we describe the QM/MM methodology for calculation of reduction and PT free energies in the two catalases. The suitability of the DFT method used for the QM part is investigated by comparing calculations on Cpd I and Cpd II cofactor models with available experimental

data. After a description of the computational details in section 3, we present in section 4 the calculated reduction free energies and the crucial 2-D free energy surfaces describing the energetics for protonation of the ferryl oxygen in the two enzymes. Thereafter, possible electron-donating residues in HPC and PVC are analyzed, and the driving force of the full reaction 4 is estimated. This work is concluded in section 5.

2. METHODOLOGY

2.1. Decomposition of the Radical Migration Reaction. The radical migration reaction 4 can be divided into a reductive half-reaction, i.e., a PT-coupled reduction of the heme from Cpd I to Cpd II

$$\text{Cpd I } (\text{Por}^{\bullet+}\text{—Fe}^{\text{IV}}\text{=O} + \text{HisH}^{+} + \text{aa}) + \text{e}^{-} \rightarrow \text{Cpd II } (\text{Por} - \text{Fe}^{\text{IV}} - \text{OH} + \text{His} + \text{aa}) \quad (5)$$

and an oxidative half-reaction involving the oxidation of an amino acid residue to form Cpd I*

$$\text{Cpd II } (\text{Por} - \text{Fe}^{\text{IV}} - \text{OH} + \text{His} + \text{aa}) \rightarrow \text{Cpd I*} \; (\text{Por} - \text{Fe}^{\text{IV}} - \text{OH} + \text{His} + \text{aa}^{\bullet+}) + \text{e}^{-} \quad (6)$$

If the protein radical cation $aa^{\bullet+}$ carries an acidic proton (as, e.g., the phenolic proton of the tyrosyl cation radical), it can relax by transferring the proton to a neighboring base (B):

$$\text{Cpd I*} \; (\text{Por} - \text{Fe}^{\text{IV}} - \text{OH} + \text{His} + \text{Tyr} - \text{OH}^{\bullet+}) + \text{B} \rightarrow \text{Cpd I*} \; (\text{Por} - \text{Fe}^{\text{IV}} - \text{OH} + \text{His} + \text{Tyr} - \text{O}^{\bullet}) + \text{BH}^{+} \quad (7)$$

Reaction 5 can be further divided into a pure one-electron reduction reaction

$$\text{Cpd I } (\text{Por}^{\bullet+}\text{—Fe}^{\text{IV}}\text{=O} + \text{HisH}^{+}) + \text{e}^{-} \rightarrow \text{Cpd II } (\text{Por—Fe}^{\text{IV}}\text{=O} + \text{HisH}^{+}) \quad (8)$$

and a PT reaction from the distal His to the ferryl oxygen

$$\text{Cpd II } (\text{Por—Fe}^{\text{IV}}\text{=O} + \text{HisH}^{+}) \rightarrow \text{Cpd II } (\text{Por} - \text{Fe}^{\text{IV}} - \text{OH} + \text{His}) \quad (9)$$

The PT-coupled reduction free energy of reaction 5, $\Delta A_{\text{red}}{}^{\text{pt}}$, is thus the sum of the pure one-electron reduction free energy of reaction 8, ΔA_{red}, and the PT free energy of reaction 9, ΔA_{pt}:

$$\Delta A_{\text{red}}{}^{\text{pt}} = \Delta A_{\text{red}} + \Delta A_{\text{pt}} \quad (10)$$

Similarly, we can combine the pure one-electron oxidation free energy of reaction 6, ΔA_{ox}, with the PT free energy of reaction 7, $\Delta A_{\text{pt}'}$, to obtain the free energy of the full oxidation reaction, $\Delta A_{\text{ox}}{}^{\text{pt}'}$:

$$\Delta A_{\text{ox}}{}^{\text{pt}'} = \Delta A_{\text{ox}} + \Delta A_{\text{pt}'} \quad (11)$$

In this work we compute the energetics of reactions 8 and 9, i.e., the energetics of the reductive half-reaction 5, for the two enzymes HPC and PVC using QM/MM calculations. The free energy of reactions 6 and 7, i.e., the energetics of the full oxidative half-reaction, $\Delta A_{\text{ox}}{}^{\text{pt}'}$, will be estimated from available experimental data. Combining the data of the two half-reactions, the free energy of the full radical migration reaction 4, ΔA, will be estimated as

$$\Delta A = \Delta A_{\text{red}}{}^{\text{pt}} + \Delta A_{\text{ox}}{}^{\text{pt}'} \quad (12)$$

2.2. Calculation of the Reduction Free Energy. The reduction free energy of reaction 8 is obtained from the linear response formula

$$\Delta A_{\text{red}} = -(\langle \Delta E \rangle_{\text{O}} + \langle \Delta E \rangle_{\text{R}}) \quad (13)$$

with ΔE being the vertical energy gap, i.e., the difference in the total potential energy of the oxidized (O) and the reduced (R) states at fixed ionic configuration:

$$\Delta E = E_{\text{O}} - E_{\text{R}} \quad (14)$$

We emphasize that ΔE is the difference between the $(N-1)$- and N-electron potential energy surfaces, not the orbital energy gap between highest occupied and lowest unoccupied molecular orbital. When calculated for an equilibrium configuration of the reduced (oxidized) state, ΔE is denoted ionization energy (electron affinity).

ΔE is sampled along a molecular dynamics trajectory in the oxidized state giving the thermal (or canonical) average of the electron affinity, $\langle \Delta E \rangle_{\text{O}}$. Similarly, sampling of the vertical energy gap in the reduced state gives the thermal average of the ionization potential, $\langle \Delta E \rangle_{\text{R}}$. Sampling of the protein dynamics is carried out with classical molecular dynamics (see details in section 3.1), whereas the vertical energy gaps are obtained from QM/MM calculations for the ensemble of configurations obtained from the classical MD runs (see details in section 3.2). Similar sampling schemes were employed in previous work.[15] Insertion of the thermal averages into eq 13 gives the absolute reduction free energy, ΔA_{red}. This procedure was carried out for both catalases HPC and PVC, yielding $\Delta A_{\text{red}}(\text{HPC})$ and $\Delta A_{\text{red}}(\text{PVC})$. The computed absolute reduction free energies cannot be directly compared to those from experiment, because the energy gaps depend on the average absolute electrostatic potential in our simulation cell, which is zero in periodic boundary conditions, but finite in experiment (due to the presence of a vapor—liquid interface). However, the relative reduction free energy of the two catalases, given by

$$\Delta\Delta A_{\text{red}} = \Delta A_{\text{red}}(\text{PVC}) - \Delta A_{\text{red}}(\text{HPC}) \quad (15)$$

does not depend on the absolute potential reference and thus can be compared to experimental data.

2.3. Calculation of the Proton Transfer Free Energy. The free energy of the water-mediated PT from the distal His to the ferryl oxygen, reaction 9, was computed by means of the metadynamics approach, originally developed by Laio and Parrinello.[16] Metadynamics is a computationally efficient method for the sampling of multidimensional free energy profiles and is becoming increasingly popular in computational chemistry[17] and biochemistry.[18] Previous applications of this method to condensed-phase chemical reactions have shown that metadynamics can yield accurate free energy profiles. For instance, we have shown for the first step of the alkaline hydrolysis of formamide in aqueous solution that metadynamics[19a] can predict the reaction barrier in good agreement with the more conventional umbrella sampling method.[19b] Metadynamics has also been successfully applied to study the molecular mechanism of Cpd I reduction by hydrogen peroxide in catalase.[20]

dx.doi.org/10.1021/ja1110706 |J. Am. Chem. Soc. 2011, 133, 4285–4298

Table 1. Experimental and Computed Fe−O Distances for Cpd I, Cpd II, and Cpd I* for Several Heme Proteins[a]

heme protein	experiment[b]	Fe=O model[c]	Fe−OH model[c]
		Cpd I	
catalase ($Tyr^-\cdots Arg^+$)	1.76 (PMC)[72]	1.62−1.66 (B3LYP)[27a,b,73]	1.78−1.80 (BP86)[6a]
	1.72 (PVC)[6a]	1.68−1.71 (BP86)[6a]	
peroxidase ($His\cdots Asp^-$) myoglobin (His)	1.65 (HRP)[74]	1.63−1.70 (B3LYP)[50,73a,75]	
		1.64 (VBP)[76]	
		1.63−1.67 (BP86)[77]	
P450 (Cys^-) CPO (Cys^-)	1.65 (CPO)[78]	1.63−1.69 (B3LYP)[50,80]	1.82 (BP86)[77b]
	1.65 (P450)[79]	1.66−1.72 (BP86)[77]	
		Cpd II/Cpd I*	
catalase ($Tyr^-\cdots Arg^+$)	1.87 (MLC)[81]	1.63−1.66 (B3LYP)[73a]	1.78−1.80 (B3LYP)[49,50,73a]
	1.82−1.85 (HPC)[6a]	1.67−1.72 (BP86)[6b], this work	1.77−1.80 (BP86)[6a,b]
		1.65 (VBP)[6c]	1.79 (VBP)[6c,d]
			1.79 (PW91)[82]
peroxidase ($His\cdots Asp^-$)		1.63−1.71 (B3LYP)[32,49,50,73a]	
	1.64/1.70/1.93 (HRP)[74,83]	1.65−1.69 (BP86)[6b,77,80a,86]	1.76−1.89 (B3LYP)[32,49,50,73a]
	1.67/1.87 (CcP)[7a,84]	1.66−1.67 (PW91)[87]	1.78−1.80 (BP86)[77,80a]
myoglobin (His)	1.88 (BpKatG)[7b,85]	1.62 (von Barth−Hedin)[86]	
	1.69/1.92 (Mb)[80a,84]	1.68 (VWN)[88]	
			1.80−1.93 (B3LYP)[80a,b,90]
P450 (Cys^-)	1.82 (CPO)[6e]	1.66−1.67 (B3LYP)[80a,b,90]	1.85 (BP86)[77]
CPO (Cys^-)	1.82 (P450)[89]	1.71 (BP86)[77]	1.83 (PW91)[82]

[a] The axial proximal ligand of the heme is indicated in parentheses. Values are given in angstroms. [b] Abbreviations used: PMC, *Proteus mirabilis* catalase; PVC, *Penicillium vitale* catalase; HRP, horse radish peroxidase; CPO, chloroperoxidase; P450, cytochrome P450; MLC, *Micrococcus luteus* catalase; HPC, *Helicobacter pylori* catalase; CcP, cytochrome *c* peroxidase; BpKatG, *Burkholderia pseudomallei* catalase peroxidase; Mb, myoglobin. [c] The exchange-correlation functional used is indicated in parentheses.

Here we use the extended Lagrangian implementation of metadynamics as described in ref 21 in combination with QM/MM. Metadynamics QM/MM runs are carried out in the space spanned by two collective variables, CV_1 and CV_2, defined in terms of coordination number differences, ΔN_{coord}. $CV_1 = \Delta N_{coord}(O_w,O;H_1) = N_{coord}(O_w-H_1) - N_{coord}(O-H_1)$ measures the degree of PT from the oxygen atom of the pocket water molecule (O_w) to the ferryl oxygen atom (O), and $CV_2 = \Delta N_{coord}(O_w,N_\varepsilon;H_2) = N_{coord}(O_w-H_2) - N_{coord}(N_\varepsilon-H_2)$ describes the PT from the N_ε atom of the distal His to O_w. The coordination number difference is defined as follows:[21,22]

$$\Delta N_{coord}(A,B;C) = N_{coord}(AC) - N_{coord}(BC) = \left[\frac{1-(r_{AC}/d_{cut})^p}{1-(r_{AC}/d_{cut})^{(p+q)}}\right] - \left[\frac{1-(r_{BC}/d_{cut})^p}{1-(r_{BC}/d_{cut})^{(p+q)}}\right] \quad (16)$$

where r_{AC} and r_{BC} are the interatomic distances, d_{cut} is a threshold distance for bonding, and p and q are exponents which determine the steepness of the decay of ΔN_{coord} with respect to r_{AC} and r_{BC}. For simulation details, we refer to section 3.3.

2.4. Performance of DFT in Describing Structural and Electronic Properties of Catalase Cpd I and II. The complex electronic structure of the intermediates of heme catalases requires a careful choice of the first-principles methodology used to describe the relevant oxidation states of the two catalases (Cpd I and Cpd II). In the following we assess the performance of DFT by comparing the results previously obtained by us and other groups concerning the structures, electronic configurations, and ionization energies of catalase and other heme enzymes with the available experimental information.

2.4.1. Structures. In Table 1 we compare the experimental Fe−O bond lengths with the computed distances for Cpd I and Cpd II of catalases and other heme proteins. The B3LYP and BP86 functionals give similar bond lengths in most cases, reproducing the available experimental values to within 0.05 Å or better. Specifically, the Fe^{IV}=O bond length of PVC catalase Cpd I is computed to be 1.68−1.71 Å at the BP86 level of theory, as compared to the experimental value of 1.72 Å. For the Fe^{IV}−OH bond of HPC Cpd I*, a bond length of 1.77−1.80 Å is obtained, compared to 1.82−1.85 Å in experiment. Thus, we conclude that the BP86 functional can reproduce both the absolute bond length and the ∼0.1 Å increase of the Fe−O bond upon proton-coupled reduction rather well.

2.4.2. Electronic Configurations and Spin States. Experimental EPR and ENDOR data[14,23] have demonstrated that Cpd I of heme enzymes can be described as an $S = 1$ Fe−O unit coupled to an $S = {}^1/_2$ porphyrin cation radical. For catalase, the coupling between the two spins is ferromagnetic (i.e., a quartet ground spin state),[14] whereas it is antiferromagnetic[23a] (i.e., a doublet ground spin state) for some peroxidases[23b] and cytochrome P450.[23c] Nevertheless, the exchange interaction is very weak, suggesting that the ground spin state is indeed a mixture of ferromagnetically (quartet) and antiferromagnetically (doublet) coupled spin states.[24] Cpd II is EPR-silent due to the disappearance of the porphyrin cation radical, and magnetic susceptibility

dx.doi.org/10.1021/ja1110706 |J. Am. Chem. Soc. 2011, 133, 4285–4298

Table 2. Relative Energies (kcal/mol) of the Low-Lying Spin States of Cpd I and Cpd II for Several Heme Proteins[a]

	Cpd I		Cpd II	
heme protein	experimental ground spin state	doublet−quartet energy splitting[b] (kcal/mol)	experimental ground spin state	singlet−triplet energy splitting[b] (kcal/mol)
catalase (Tyr^-)	quartet[14]	+0.6 (BP86)[20] −0.3, −0.05 (B3LYP)[27b,51a]	triplet[6c,d,25]	+10.8 (BP86)[c]
HRP (His)	doublet[23a] + quartet[24]	−0.2, +0.7 (B3LYP)[51a,75b]	triplet[25]	+11.4 (B3LYP)[32] +10.7 (B3P86)[32] +16.5 (MPW1K)[32]
P450 (Cys^-)	doublet[23c]	0.0 (BP86)[91] −3.0 (BPW91)[92] −0.04, −0.3 (B3LYP)[80c,93] −1.8, −0.6 (CASSCF, CASPT2)[93,94]	triplet[78]	
CPO (Cys^-)	doublet[23b]	−0.15 (B3LYP)[95] −0.9 (CASPT2)[94]	triplet[78]	

[a] The axial proximal ligand of the heme is indicated in parentheses. A positive energy splitting means a quartet Cpd I or a triplet Cpd II ground spin state. [b] The DFT exchange-correlation functional or the multireference method used is indicated in parentheses. [c] This work.

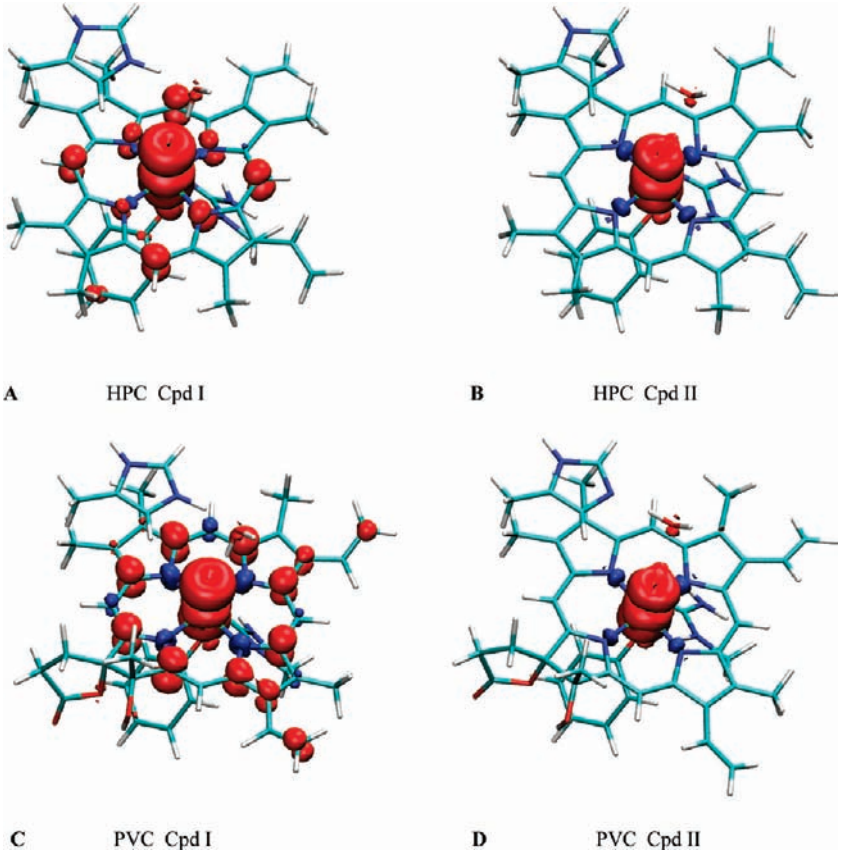

Figure 2. Calculated spin density distributions for catalase Cpd I and Cpd II: (A) HPC Cpd I, (B) HPC Cpd II, (C) PVC Cpd I, (D) PVC Cpd II. Spin isodensity surfaces are plotted at −0.004 e $Å^{-3}$ (red) and 0.004 e $Å^{-3}$ (blue).

measurements indicate an $S = 1$ Fe−O unit with a triplet ground spin state.[25] EPR and ENDOR spectra show that Cpd I* contains an $S = 1$ Fe−O unit coupled to an $S = {}^1/_2$ tyrosyl or tryptophanyl radical.[14b,26]

In Table 2 we summarize electronic structure calculations carried out for Cpd I and II in several heme enzymes using the BP86 and B3LYP density functionals, as well as multireference methods. We focus our discussion on the results obtained with the functional used in this work (BP86). The electronic configuration and ground spin state of catalase Cpds I and II[6a,b,27] are in agreement with those from experiment. Specifically, catalase Cpd I shows three unpaired electrons (Figure 2A,C), two located on the Fe−O moiety and the other delocalized over the porphyrin ring, that couple ferromagnetically, yielding a quartet ground spin state. Upon one-electron reduction (Cpd II), the unpaired spin density on the porphyrin disappears (Figure 2B,D) due to the reduction of

dx.doi.org/10.1021/ja1110706 |J. Am. Chem. Soc. 2011, 133, 4285–4298

the porphyrin cation radical, and thus, the ground spin state becomes a triplet. In other words, the HOMO of the porphyrin is half-filled in Cpd I and doubly occupied in Cpd II. Moreover, BP86 predicts that the doublet−quartet spin splitting of Cpd I is very small, in line with experimental evidence showing that the ferromagnetic coupling is very weak in catalase.[14b]

2.4.3. Electron Affinities, Ionization Energies, and Proton Transfer Energies. The performance of DFT in predicting the ionization energies of porphyrins was tested by the groups of Ghosh[28] and Scheiner.[29] It was found that the BP86 results[30] are in good agreement with the electrochemical data, with errors of ≤0.15 eV for absolute ionization potentials and ≤0.05 eV for electron affinities. We expect similar if not smaller errors for the *relative* ionization potentials between the different porphyrin cofactors investigated in this study.

There is no experimental information available on proton transfer energies involving an oxoferryl···water···histidine system. However, benchmark calculations on Truhlar's PA8 database of proton affinities of small molecules give a mean unsigned error of 0.06 eV for BP86,[31] showing that this functional is expected to describe the thermodynamics of the PT reaction well. It is worth mentioning that the water-mediated PT from the distal His to the ferryl oxygen found here for HPC was also described for Cpd II of another heme b-containing hydroperoxidase, horseradish peroxidase (HRP).[32] Even though both proteins have different axial ligands (tyrosinate in HPC and histidine in HRP), the QM(DFT/B3LYP)/MM potential energy surface for HRP Cpd II gave a large stabilization upon protonation of the ferryl oxygen (by 0.46 eV), similarly to what we report for HPC (see section 4.2).

3. SIMULATION DETAILS

3.1. Classical MD. The starting points of the present simulations are the X-ray structures of HPC (PDB code 2IQF) and PVC (PDB code 2IUF). They include the complete tetrameric proteins, shown in Figure 1A,B. The oxidation and protonation states of the active site in each of the four catalase subunits is shown in Figure S1, Supporting Information. In the oxidized (O) state, all the hemes were considered to be in the Cpd I configuration, whereas in the reduced (R) state only the heme in subunit A was reduced to the Cpd II state. In both oxidation states the oxoferryl group is unprotonated (i.e., Fe═O). The distal His is protonated in protein subunits A and C and neutral in B and D. Conventional (pH 7) protonation states were chosen for all residues. The protonation state of the histidine residues took into account their hydrogen bond environment, and all aspartates and glutamates were taken as deprotonated to carboxylate anion, except when there was a close contact between two acidic residues. The proximal tyrosines (339 in HPC and 351 in PVC) were taken as deprotonated. A total of 3.5 sodium ions per subunit of HPC and 9 per subunit of PVC were added to neutralize the protein structure. The system was enveloped in a box of equilibrated TIP3P water molecules with volume 110.1 Å × 123.3 Å × 129.6 Å for HPC and 128.9 Å × 125.7 Å × 167.6 Å for PVC. The total size of the system is 155541/244608 atoms, respectively (31858/42238 protein and heme atoms + 123683/202370 water and counterion atoms).

The parameters employed for protein residues, the heme b in HPC, and the heme d of PVC were the same as in our previous work on catalase Cpd I.[6a] Only the parameters describing the interaction between Fe and its ligands were slightly modified. The equilibrium bond lengths and angles were substituted for those obtained in the QM/MM geometry optimizations of catalase Cpd I and Cpd II, and the Fe═O force constant was re-estimated from a short QM/MM molecular dynamics simulation for catalase Cpd I.[6a] Atomic RESP charges were parametrized as follows. The QM/MM-optimized geometries of Cpd I and Cpd II[6a] were used to build a simplified model comprising the heme (as a porphyrin without substituents, except the *cis*-hydroxy-γ-spirolactone in heme d), the proximal Tyr and Arg (phenolate and methylguanidium), a water molecule, and the distal His (methylimidazolium). The valences were saturated with hydrogen atoms. Their positions were optimized with the Gaussian program[33] at the BP86/6-31++G** level, whereas the rest of the structure was kept at the CPMD QM/MM geometry. ESP charges were obtained at the BP86/6-31++G** level, and the final RESP charges were fitted using the Antechamber program[34] of the AMBER package.[35] The final parameters of the O and R states are identical, except for the RESP charges of the active site in subunit A (i.e., modeling Cpd I in the O state and Cpd II in the R state).

The solvated O state was equilibrated in several steps. First, all water molecules and counterions were relaxed with a gradient minimizer, and then the protein was also minimized. Next, the solvent was equilibrated for 400/600 ps (HPC or PVC, respectively) at 150 K (protein constrained), followed by an equilibration of the protein at the same temperature for 200/200 ps. After equilibration at 150 K, the system was equilibrated at 300 K for 1.0/2.5 ns by coupling to a heat bath at the desired temperature. The system was equilibrated for 10 ns at 300 K and constant pressure by coupling to a heat bath and a Berendsen barostat, respectively. The following 10 ns of classical dynamics were taken for QM/MM calculation of configurational averages ($\langle \Delta E \rangle_O$; see section 2.2). The MD simulation of the R state was started using as the initial geometry a snapshot of the O state after 2 ns of equilibration in the NPT ensemble. After equilibration for 10 ns, the following 10 ns were taken for the QM/MM calculation of $\langle \Delta E \rangle_R$. During both runs, the center of mass of each subunit was constrained to the initial value with a harmonic force constant of k = 5 kcal mol^{-1} Å^{-2} to avoid rotation of the entire protein complex, which would bring protein atoms too close to the boundary of the cubic unit cell. Analysis of the trajectories was carried out using standard tools of AMBER[35] and VMD.[36]

3.2. QM/MM Energy Gaps. The QM/MM model used for the calculation of the energy gaps in eq 14 and reduction free energy in eq 13 is illustrated in Figure 3. The QM region is comprised of the heme ring, the axial ligand Tyr339/351, the proximal Arg335/347, the distal His56/64, and the pocket water molecule bridging the ferryl oxygen and His56/64. The QM region is contained in a box of dimensions 16.88 × 20.00 × 18.83 Å^3 for HPC and 20.90 × 19.73 × 20.79 Å^3 for PVC. The QM−MM boundary was saturated with "dummy" hydrogen atoms located at His56/64, Tyr339/351, Arg335/347, and the two heme b or the one heme d propionates. As discussed in the Supporting Information (Table S1 and Figure S2), this QM model (model 5 in the Supporting Information) reproduces the electronic distribution observed in EPR experiments and is sufficiently large for converging the calculations of the energy gap in eq 14.

QM/MM calculations were performed using the CPMD package[37] in combination with the Amber99 force field used in the classical MD simulation. Norm-conserving Troullier−Martins pseudopotentials were used to describe the nuclei and core electrons of the QM atoms. For iron, a 16 valence electron

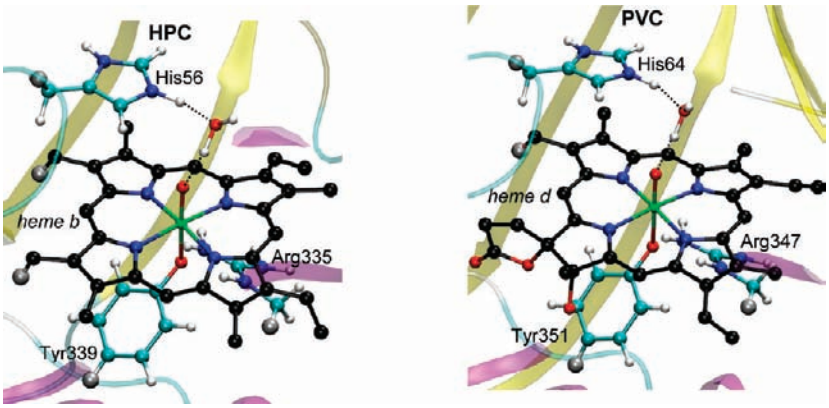

Figure 3. QM−MM partition used in the calculation of the vertical ionization energies of Cpd I and Cpd II in HPC and PVC. The QM region is shown in ball and stick representation, and the link atoms are colored in silver. Hydrogen atoms of the heme group are omitted for clarity.

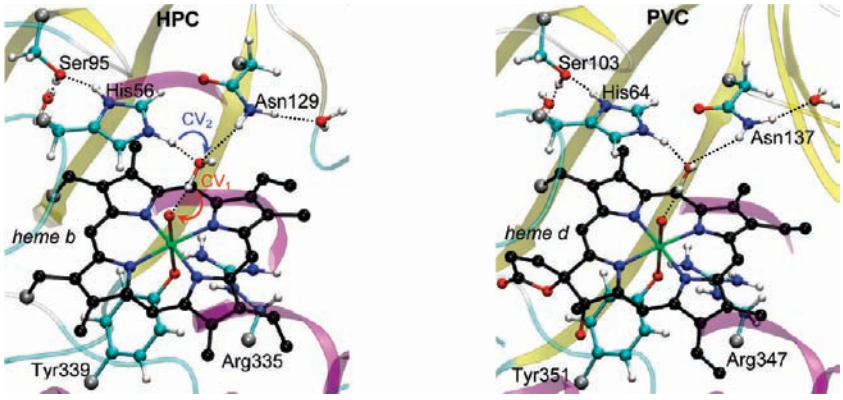

Figure 4. QM−MM partition and reaction coordinates (CV_1 and CV_2) used in the metadynamics simulation of the PT from the distal His to the ferryl oxygen in HPC and PVC. The QM region is shown in ball and stick representation, and the link atoms are colored in silver. Hydrogen atoms of the heme group are omitted for clarity.

semicore pseudopotential was used. For all other atoms well-tested valence pseudopotentials were used, as specified in refs 6a and 6b. The electronic orbitals were expanded in plane waves using a reciprocal space kinetic energy cutoff of 90 Ry. The exchange-correlation functional was calculated according to Becke and Perdew (BP86).[38] A similar setup was successfully employed in several previous DFT studies of heme enzymes.[6a,b,20,39] The electrostatic interaction energy between the QM and MM regions was calculated by real space integration of the Coulomb interaction between all MM atoms within a distance r_{NN} = 5.3 Å of any QM atom and the full electron + nuclei density of the QM subsystem.[40] Table S2, Supporting Information, shows that the energy gap in eq 14 is converged for this choice of the r_{NN} cutoff radius. All other MM atoms interact with the QM atoms using the RESP charges assigned to the QM atoms.[41] Long-range electrostatic interactions between MM atom pairs are described by Ewald summation using the P3M implementation[42] and a 256 × 256 × 256 mesh.

The vertical energy gap in eq 14 was calculated at the QM/MM level of theory on n = 21 equidistantly spaced snapshots extracted from the classical MD simulations of the oxidized (O) and the reduced (R) states for each catalase (HPC and PVC) (see section 3.1) to compute the thermal averages $\langle \Delta E \rangle_O$ and $\langle \Delta E \rangle_R$ in eq 13. Table S3, Supporting Information, shows that the average and the width of the thermal fluctuations of ΔE are converged for the sampling density (i.e., the time interval between two classical MD snapshots) used in the final calculations, 0.5 ns. The statistical uncertainty of the energy gap calculations, $\sigma/n^{1/2}$, where σ is the root-mean-square fluctuation of the energy gap, is 0.06 eV for both HPC and PVC.

3.3. QM/MM Metadynamics. Calculations of PT free energies were performed on a slightly larger QM model that is shown in Figure 4 (denoted QM model 8 in the Supporting Information). Compared to model 5 used for the calculation of the reduction free energy, it additionally includes the distal serine and asparagine residues (Ser95/103 and Asn129/137) and two water molecules hydrogen-bonded to these residues. The hydrogen bond between Ser and the distal His is expected to influence the pK_a of the imidazole group, whereas the hydrogen bond between Asn and the pocket water may affect the polarization of the water O−H bonds. The electronic structure method (DFT/BP86) is the same as described above. We found that the oxoferryl (Fe═O) form of HPC Cpd II is not stable against thermal fluctuations and the PT occurs spontaneously, yielding the hydroxoferryl (Fe−OH) configuration. Hence, the simulation in HPC was initiated from the product, Fe−OH. In contrast, the Fe═O form of PVC Cpd II is stable, and thus, the simulation was initiated from the oxoferryl reactant structure. Starting from the optimized geometries of HPC Fe−OH Cpd II and PVC Fe═O Cpd II, standard Car−Parrinello QM/MM molecular dynamics simulation at room temperature was performed first to equilibrate the system (∼ 1.7 ps for HPC and ∼2.7 ps for PVC).

dx.doi.org/10.1021/ja1110706 |J. Am. Chem. Soc. 2011, 133, 4285–4298

The following parameters were used: δt = 0.12 fs (time step), μ_e = 700 au (fictitious electronic mass of the CP Lagrangian), ν = 650 cm^{-1} (frequency of the Nosé−Hoover thermostat). Then, metadynamics QM/MM simulations were initiated using the two collective variables defined in section 2.3 and eq 16; see Figure 4 for an illustration. The values for the threshold distance (d_{cut}) and the exponents (p and q) for the coordination numbers are given in Table S4, Supporting Information. The parameters for metadynamics, that is, the mass of the fictitious particle (M) and the force constant (k) coupling the fictitious particle to the real system, as well as the height (w) and the width (δs) of the Gaussian history-dependent potential, are also summarized in Table S4. A new Gaussian potential "hill" was added every 150 MD steps (i.e., 18 fs). A total of about 230/150 Gaussian hills were added for HPC/PVC, respectively, to fully explore the 2D free energy profile. In terms of simulation time, this corresponds to ~3.5 × 10^4/~2.3 × 10^4 MD steps (~4.1/~2.7 ps). The metadynamics simulations were stopped once recrossing to the initial state was observed. The error for the obtained PT free energy is expected to be of the same order as the resolution of the hills being used (1 kcal/mol for HPC and 0.5 kcal/mol for PVC).

4. RESULTS AND DISCUSSION

4.1. Pure One-Electron Reduction Potential of Cpd I. In a first set of simulations, we have investigated the free energy for pure one-electron reduction of the heme active site of Cpd I of HPC and PVC, reaction 8. The vertical energy gaps in eq 14 are obtained from QM/MM calculations on protein configurations sampled with classical MD, as described in section 3.1. The thermal fluctuations of the energy gaps are shown in Figure 5 for HPC and PVC. The energy for vertical insertion of an electron into Cpd I (electron affinity, solid lines) fluctuates around 5.5 eV for both proteins, whereas the energy for vertical removal of an electron from Cpd II (ionization energy, dashed lines) fluctuates around 7.2 eV. The difference between electron affinity and ionization potential is a signature of the different protein and solvent structures in the two oxidation states. Taking the thermal averages and inserting them into eq 13, we obtain the free energy for pure one-electron reduction, ΔA_{red}, for the two catalases. The difference in eq 15, which can be compared to experiment, is very small, $\Delta\Delta A_{red}$ = 0.03 eV. This is less than the statistical error of our calculations (0.06 eV; see section 3.2).

The almost negligible difference in reduction potential is not unexpected because experimental $Fe^{3+/2+}$ reduction potentials of other heme b- and d-type proteins also fall within a similar range.[43] A breakdown of the total reduction free energy into contributions from the heme (*inner-sphere*) and the protein and solvent (*outer-sphere*) regions, $\Delta\Delta A_{red} = \Delta\Delta A_{red}^{i} + \Delta\Delta A_{red}^{o}$, gives $\Delta\Delta A_{red}^{i} = -0.09 \pm 0.06$ eV and $\Delta\Delta A_{red}^{o} = 0.12 \pm 0.06$ eV. Thus, the intrinsic propensity for reduction of the heme ($\Delta\Delta A_{red}^{i}$) is slightly larger for the heme d ring, in line with the 10−320 meV higher reduction potentials of synthetic chlorins (similar to heme d) compared to synthetic porphyrins (similar to heme b).[44] On the contrary, the outer-sphere contribution due to the protein and solvent ($\Delta\Delta A_{red}^{o}$), albeit small, has an opposite sign, shifting the total difference close to zero. Therefore, our calculations suggest that the different propensities for radical migration in Cpd I of HPC and PVC are not caused by differences in pure one-electron reduction free energies of the heme b and heme d rings, respectively.

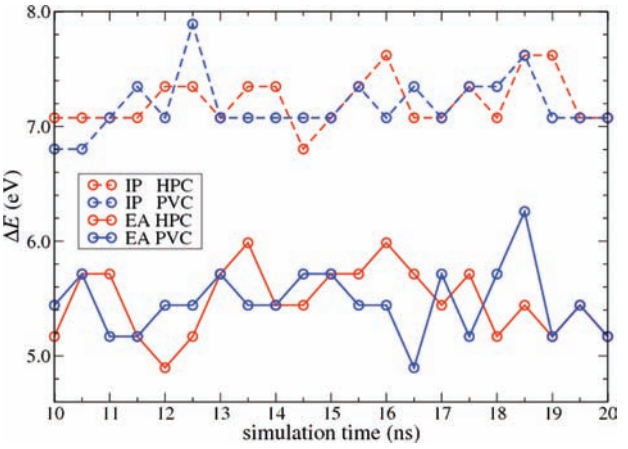

Figure 5. Fluctuations of the vertical energy gap ΔE (eq 14) at 300 K for the pure one-electron reduction of the heme Cpd I to Cpd II, reaction 8.

4.2. Proton Transfer Free Energies for Cpd II. In a second series of simulations we have computed the free energy for PT from the protonated distal His56/64 (HPC/PVC residue notation) to the ferryl oxygen atom of Cpd II, reaction 9. In both enzymes His56/64 is not directly hydrogen bonded to the ferryl oxygen but via a crystal water molecule (see Figure 4), which is very stable against thermal fluctuations and well positioned to mediate the PT. We have chosen two collective variables (CVs) to describe the water-mediated PT, as indicated in Figure 4A (see details in section 3.3). CV_1 describes the PT from the water molecule to the ferryl oxygen and CV_2 the PT from the distal His to the pocket water. A 2-D free energy surface (FES) along these coordinates was mapped out using QM/MM metadynamics calculations.

The FES obtained for HPC is displayed in Figure 6, left panel. There is one single pathway connecting the reactants (Por—Fe^{IV}=O + $HisH^+$) to the products (Por−Fe^{IV}−OH + His). It shows two degenerate minima, R and R*, corresponding to the reactant state of Cpd II (Por—Fe^{IV}=O + $HisH^+$). Going from R to R* the hydrogen bonds O−H_1 and O_w−H_2 shorten, generating the polarization required for the break of the O_w−H_1 bond at the TS. After the TS is reached, the H_1 proton is fully transferred from the pocket water to the oxoferryl group, generating a transient hydroxide species that is immediately quenched to water by transfer of the H_2 proton from the distal $HisH^+$. The resulting product state, Cpd II (Por−Fe^{IV}−OH + His), is represented by two minima, P and P*, differing in the hydrogen bond pattern of the crystal water. The active site structures corresponding to the stationary points of the free energy surfaces are given in the Supporting Information (Figure S3). From the energetic point of view, the barrier for PT is small, about 0.09 eV, whereas the reaction free energy, ΔA_{pt}, is large and negative, −0.65 ± 0.04 eV. Thus, reaction 9 is predicted to occur with a high driving force in HPC. This is in agreement with a previous experimental study on *Proteus mirabilis* catalase (PMC), a heme b-containing catalase similar to HPC, showing that protonation of the oxoferryl group of Por—Fe^{IV}=O is irreversible.[6c,d]

The corresponding FES for PVC is shown in Figure 6, right. Two main differences are noticeable when compared to the FES of HPC. First, both covalent bonds O_w−H_1 and N_ε−H_2 are broken in the TS, and the two protons H_1 and H_2 are transferred

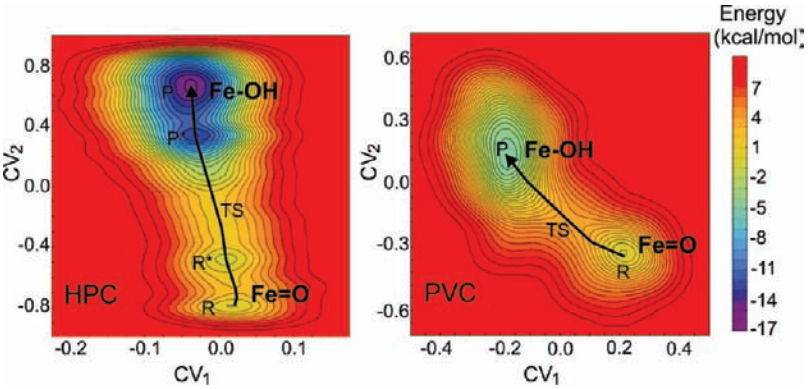

Figure 6. 2-D free energy surfaces corresponding to proton transfer from the distal histidine to the ferryl oxygen, reaction 9, for HPC and PVC.

Table 3. pK_a Values of the Distal Histidine, pK_a(HisH$^+$), in Several Hydroperoxidases[a]

heme redox state	BLC	ANC	HRP
Cpd I	≤5.5[b]	6.1[d]	5.0[f]
Cpd II	8.0[c]	na[e]	8.6[f]

[a] Abbreviations: HRP, horseradish peroxidase; BLC, bovine liver catalase; ANC, *Aspergillus niger* catalase. [b] Estimated from the pH profile of the inhibition of catalase Cpd I by 3-aminotriazole in BLC and ANC.[96] [c] From ref 97. [d] From ref 96b. [e] The pK_a of the distal His in Cpd II of large subunit catalases (such as ANC or PVC) cannot be estimated because these catalases are apparently not reduced to Cpd II.[98] [f] From ref 47.

almost simultaneously (see Figure S4, Supporting Information), in contrast to HPC, where the proton transfer happens in a more sequential fashion.[45] Second, the barrier for PT is slightly larger, 0.15 eV. Third and most strikingly, the reaction free energy is only $\Delta A_{pt} = -0.19 \pm 0.02$ eV. Thus, reaction 9 is significantly less exergonic in PVC than in HPC, by $\Delta\Delta A_{pt} = \Delta A_{pt}(\text{PVC}) - \Delta A_{pt}(\text{HPC}) = 0.46 \pm 0.04$ eV. As we will argue further below, this large difference in the driving force for PT in Cpd II is likely to be the main reason for the different propensities of radical migration in the two enzymes.

The free energy for PT from the distal His to the oxoferryl can be written in terms of the pK_a difference between these two groups:

$$\begin{aligned}\Delta A_{pt} &= 0.059\Delta pK_a \\ &= 0.059[pK_a(\text{HisH}^+) - pK_a(\text{Fe}-\text{OH})] \end{aligned} \quad (17)$$

Therefore, the larger driving force in HPC may be due to a lower pK_a of the distal His and/or a higher pK_a of the hydroxoferryl compared to PVC. Table 3 shows the pK_a of the distal His of three hydroperoxidases: bovine liver catalase (BLC; a small subunit catalase similar to HPC), *Aspergillus niger* catalase (ANC; a large subunit catalase similar to PVC), and horse radish peroxidase (HRP).[46] The distal His in ANC Cpd I is slightly more basic (6.1) than in BLC (5.5), and thus, it is reasonable to think that the pK_a of the distal His in PVC Cpd I will also be higher than in HPC. The basicity of the distal His in BLC Cpd II is higher (8.0) than in Cpd I (5.5). This effect of the oxidation state of the heme in the pK_a of the distal His was also observed for HRP.[47] Although there are no experimental data for Cpd II of any heme d-containing catalase, our previous results on the catalase reaction[20] suggest that the distal His is also more basic in PVC Cpd II than in HPC. Even though we could not estimate the pK_a, we showed that the different pK_a values of the distal His in HPC and PVC are probably due to a combined effect of the protein environment and not due to the different types of heme. This is in line with both BLC and HRP containing heme b but having different p$K_a$values (HisH$^+$) (see Table 3). However, assuming the difference in pK_a(HisH$^+$) between HPC and PVC Cpd II is the same as that in Cpd I (6.1 − 5.5 = 0.6 pK_a units), the contribution of the distal His to $\Delta\Delta A_{pt}$ would be only 0.03 eV. Therefore, the main determinant of the different energetics of the PT is the oxoferryl group being more basic in HPC than in PVC.

The pK_a of heme b-containing catalases, such as PMC or HPC, is not precisely known due to the difficulty in characterizing the Fe−OH band in the RR spectrum (see the discussion in ref 48) and the lack of EXAFS and RR experiments at acidic pH.[49] The pK_a of the oxoferryl group in catalase has been proposed[49] to be an intermediate case between thiolate-ligated enzymes (such as chloroperoxidase (CPO) and cytochrome P450) and imidazole-ligated heme proteins (such as hemoglobin (Hb), myoglobin (Mb), HRP, and cytochrome *c* peroxidase (CcP)). The larger basicity of the oxoferryl group for thiolate-ligated heme proteins compared to imidazole-ligated heme proteins[49,50] has been explained by a larger π donation from the anionic cysteinate compared to the neutral imidazole.[6d,e] In catalases the negative charge of tyrosinate ligand is partially counteracted by a nearby arginine, and thus, the pK_a(Fe−OH) is lower than for thiolate-ligated heme proteins, but still higher than for imidazole-ligated heme proteins. Similarly, we propose that the larger basicity of the ferryl oxygen in HPC compared to PVC may be explained qualitatively, in terms of a simple orbital picture. Reduction from Cpd I to Cpd II is essentially the insertion of an electron into the LUMO of the porphyrin. This orbital has A_{2u} symmetry in HPC (i.e., it has nodes in the pyrrole nitrogens and the meso carbons; see Figure 2A)[6a] and A_{1u} symmetry in PVC (i.e., it has nodes in the pyrrole carbon atoms; see Figure 2C). As the A_{2u} orbital mixes more effectively with the π system of the proximal tyrosinate ligand, the electron density in HPC Cpd II is increased on the Fe−Tyr bond and, due to the push−pull effect,[51] also on the Fe−O bond. This results in a more negatively charged oxoferryl group in HPC and thus a higher proton affinity.

4.3. Electron-Donating Protein Residue. For a complete description of radical migration (eq 4), it is necessary to investigate possible amino acids that can reduce Cpd I. HPC and PVC Cpd I have not been characterized by EPR spectroscopy yet, and therefore, the location of the possible protein radical is not known. However, the type and location of the protein radical are known for other catalases. A tyrosyl radical has been detected for bovine liver catalase (BLC) at Tyr369.[9a] On

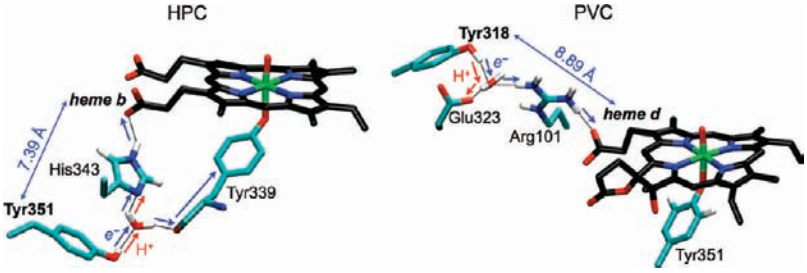

Figure 7. Proposed tyrosyl radical sites in HPC (Tyr351) and PVC (Tyr318). The distance and the possible ET pathways (blue arrows) from the tyrosine residue to the heme, as well as the possible PT pathways (red arrows) from the tyrosyl radical to the proton acceptor (His343 in HPC and Glu323 in PVC), are also shown.

the basis of sequence alignment and the similarity of the local structure environment compared to BLC, a tyrosine (Tyr370) was also proposed to form a protein radical in the human erythrocyte catalase (HEC).[9b]

To analyze possible electron-donating residues in HPC and PVC, we took into account the following selection criteria: (i) Only Tyr and Trp residues are considered as possible radical sites in Cpd I*, as most protein radicals detected in oxidized heme proteins correspond to either of these amino acids.[52] (ii) Only residues within 14 Å of the edge of the heme ring are considered, since direct electron tunneling at a significant rate is thought to be limited to this distance.[53] (iii) The electron transfer is favored if the electron-donating residue is connected via a hydrogen bond path to the heme, or to axial iron ligands, because electrons tunnel along hydrogen bonds faster than through a vacuum.[54] (iv) The electron-donating residue should form a hydrogen bond either directly or indirectly via a relay to a proton acceptor to stabilize the acidic tyrosyl or tryptophan radical cation by PT.[52]

According to our analysis of the crystal structure of HPC, there are 18 possible candidates that fulfill criteria i and ii (12 Tyr and 6 Trp residues). Of these residues, we believe that HPC Tyr351 is the most likely electron donor for the following reasons. It is the closest to the heme b cofactor (7.39 Å), and it is well connected to the latter by two ET pathways (see Figure 7 , left, for an illustration). One pathway leads from the phenyl ring of Tyr351 to the water molecule hydrogen bonded to it and further on to the carbonyl group of the proximal Tyr339 that coordinates the Fe ion. A similar pathway was suggested for HEC[9b] and for the P450−putaredoxin complex.[55] The other pathway leads from the water molecule hydrogen bonded to Tyr351 to His343 and further on to one of the propionate side chains of the heme group. A similar electron tunneling pathway was proposed for ascorbate peroxidase (APX).[56] In addition to providing an electronic conduit, the water molecule connecting Tyr351 with His343 could also act as a relay for the proton transfer from the highly acidic tyrosine radical cation ($pK_a = -2$)[57] to His343. Thus, Tyr351 fulfills all the selection criteria listed above. Moreover, Tyr351 is equivalent to Tyr369 of BLC and to Tyr370 of HEC, both of which were shown to be the radical site in Cpd I*.[9,14a]

Similar considerations hold for PVC. There are 4 Tyr and 3 Trp residues within 14 Å of the heme group. Among them, Tyr318 is the electron-donating amino acid closest to the heme d group (8.89 Å; see Figure 7 , right), and it is connected to the heme by a hydrogen bond pathway that leads from the phenyl ring of Tyr318 via a water molecule to Arg101 and one of the propionate groups of the heme, thus providing a reasonable ET pathway, in terms of both distance and efficiency.[54a,58] Moreover, the resulting tyrosyl cation radical can be deprotonated by a nearby glutamate (Glu323) via the water molecule. A similar deprotonation pathway has been proposed for the bacterial photosynthetic reaction center.[59] On the basis of these arguments, we propose that Tyr318 is the most likely electron donor in PVC Cpd I.

4.4. Proton-Coupled Oxidation Free Energies. As shown in eq 11, the reaction free energy for the PT-coupled oxidation of Tyr351/318, $\Delta A_{ox}^{pt'}$, can be estimated as the sum of the pure one-electron oxidation free energy of TyrOH to $TyrOH^{\bullet+}$, ΔA_{ox}, and the free energy for PT from $TyrOH^{\bullet+}$ to the proton acceptor (His343 for HPC and Glu323 for PVC):

$$\begin{aligned}\Delta A_{pt'} &= 0.059\Delta pK_a \\ &= 0.059[pK_a(TyrOH^{\bullet+}) - pK_a(B)] \end{aligned} \quad (18)$$

Taking the experimental data for oxidation free energy and pK_a values in aqueous solutions, ΔA_{ox} = 1.44 eV (vs NHE) for tyrosine,[60] and $pK_a = -2$, 6.15, and 4.5 for the tyrosyl radical cation, histidine, and glutamic acid, respectively,[57,61] we obtain PT-coupled oxidation free energies ($\Delta A_{ox}^{pt'}$) of 0.96 and 1.06 eV (vs NHE) for HPC and PVC, respectively.

The values obtained for $\Delta A_{ox}^{pt'}$ are approximate since they have been estimated by using experimental data for aqueous solutions, not for the protein environment. Therefore, it is worth trying to quantify the uncertainty of this estimation. The oxidation free energy of tyrosine may be affected by ~0.1 eV due to the change in hydrogen-bonding to the phenolic proton.[62] Hydrogen-bonding to a proton-accepting amino acid decreases $\Delta A_{ox}^{pt'}$,[63] and this shift is expected to be larger for HPC than for PVC because His343 is a stronger base than Glu323.[63b] Besides, the pK_a of the proton acceptor may also change due to protein electrostatic interactions. The pK_a of His343 in HPC is probably higher due to the hydrogen-bonding to the negatively charged heme propionate, lowering $\Delta A_{pt'}$. For instance, in photosystem II, the histidine residue acting as a proton acceptor in the oxidation of tyrosine is hydrogen-bonded to a glutamate, and its pK_a is 7.5,[64] i.e., a −0.08 eV shift compared to that in solution. On the other hand, the pK_a of Glu323 in PVC is expected to be lowered by the salt bridge to Arg101, raising $\Delta A_{pt'}$ by ~0.01[65] to 0.02[66] eV.[67] Considering all these factors, the PT-coupled oxidation free energies ($\Delta A_{ox}^{pt'}$) are 0.96 ± 0.15 and 1.06 ± 0.15 eV (vs NHE) for HPC and PVC, respectively.

The free energy difference between the two catalases, $\Delta\Delta A_{ox}^{pt'} = \Delta A_{ox}^{pt'}(PVC) - \Delta A_{ox}^{pt'}(HPC)$, is thus 0.10 eV. Interestingly, this difference is due to the different pK_a values of the proton acceptors (His343 of HPC and Glu323 of PVC). Therefore, the main determinant of the different energetics of

dx.doi.org/10.1021/ja1110706 |J. Am. Chem. Soc. 2011, 133, 4285–4298

Table 4. Summary of Computed and Experimental Reduction, Oxidation, and Proton Transfer Free Energies for HPC and PVC[a]

free energy component	HPC	PVC	PVC − HPC
ΔA_{red} [b]	−0.23 ± 0.04	−0.20 ± 0.04	**0.03 ± 0.06**
ΔA_{pt} [c]	**-0.65 ± 0.04**	**-0.19 ± 0.02**	**0.46 ± 0.04**
ΔA_{red}^{pt} [d]	−0.88*	−0.39 ± 0.07	**0.49 ± 0.07**
$\Delta A_{ox}^{pt'}$ [e]	0.96*	1.06*	0.10*
ΔA[f]	0.08	0.67 ± 0.07	0.59 ± 0.07

[a] Values in bold font were obtained directly from QM/MM calculations (sections 4.1 and 4.2), values marked with an asterisk were estimated from experimental data (sections 4.4 and 4.5), and all other values were obtained by combining computed and experimental data. All values are given in electronvolts. [b] Reaction 8 and eq 13. [c] Reaction 9. [d] Reaction 5 and eq 10. [e] Reactions 6 and 7 and eq 11. [f] Reaction 4 and eq 12.

tyrosine oxidation is the proton acceptor being more basic in HPC than in PVC.

4.5. Reaction Free Energy of Radical Migration into the Protein (Reaction 4). Table 4 summarizes the data for the reductive half-reaction obtained from QM/MM calculations in sections 4.1 and 4.2 (bold font) and the data for the oxidative half-reaction obtained from experimental data in section 4.4 (marked with an asterisk). Combining all data, we can calculate the difference in the driving force for protein radical migration in HPC and PVC, reaction 4:

$$\Delta\Delta A = \Delta\Delta A_{red}^{pt} + \Delta\Delta A_{ox}^{pt'} \quad (19)$$

where $\Delta\Delta A = \Delta A(\text{PVC}) - \Delta A(\text{HPC})$. We obtain $\Delta\Delta A = 0.59 \pm 0.07$ eV (where we include the statistical error due to the computation of $\Delta\Delta A_{red}^{pt}$ only), showing that radical migration in HPC is significantly favored as compared to that in PVC, in agreement with the experimental findings.[6a] In addition, we show that the main factor contributing to this difference is the free energy for proton transfer from the distal His to reduced Cpd I ($\Delta A_{pt} = 0.46 \pm 0.04$ eV).

While the relative free energy difference in 19 is a measure of the tendency to form a protein radical among different enzymes, it does not give information as to whether a protein radical is actually formed. This information is given by the absolute ET free energy for each protein, ΔA. The computation of this quantity would require the calculation of energy gaps for tyrosine oxidation using QM/MM, with the corresponding free energy to be added to the free energy for Cpd I reduction. This calculation is fraught with technical problems and is likely to be inaccurate, in particular due to the different dependences of the energy gaps with respect to the QM size chosen for the oxidative and reductive half-reactions.

Alternatively, we relate here the computed QM/MM reduction free energies to the experimental redox potential scale by assuming that ΔA_{red}^{pt} of HPC is equal to the experimental value for another heme b-containing hydroperoxidase, HRP,[68] with $\Delta A_{red}^{pt} = -0.88$ eV vs NHE (note the negative value for the reduction free energy as opposed to the positive reduction potential of HRP). Using this value together with the calculated values for the reductive half-reaction and the data for the oxidative half-reaction, one can construct a free energy profile vs NHE for the single reaction steps that constitute radical migration in HPC and PVC (Figure 8).

As illustrated in Figure 8, the pure one-electron reduction of Cpd I to Cpd II is favorable with respect to NHE ($\Delta A_{red} < 0$) by

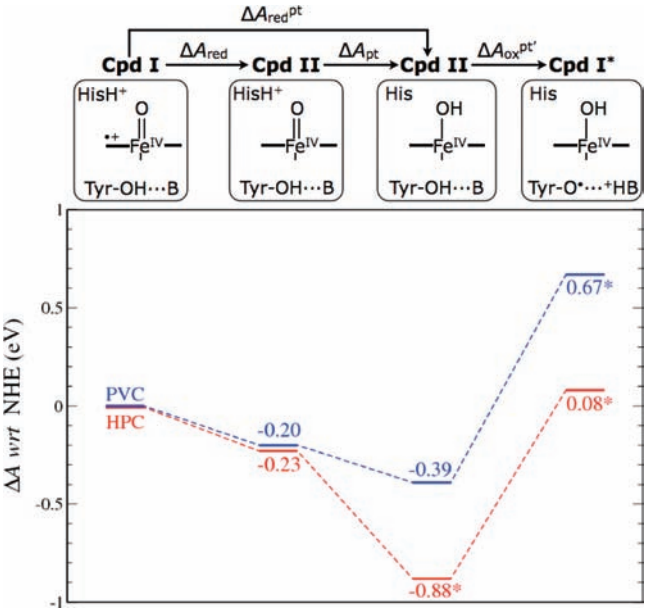

Figure 8. Comparison of the free energy profile (vs NHE) for radical migration in HPC (red) and PVC (blue). The free energy of HPC Cpd II (Fe−OH) was set equal to the experimental reduction free energy of HRP Cpd I vs NHE, −0.88 eV. Energy levels denoted by an asterisk are estimated from experimental data; all other energy levels were obtained from QM/MM computations. Data are taken from Table 4.

about 0.2 eV, and the difference between HPC and PVC ($\Delta\Delta A_{red} = 0.03$ eV) is negligibly small, as noted in section 4.1. PT from the distal His to the ferryl oxygen of Cpd II further lowers the free energy ($\Delta A_{pt} < 0$) in both enzymes, but the reaction is much more exergonic for HPC ($\Delta\Delta A_{pt} = 0.46$ eV), as noted in section 4.2. The PT-coupled oxidation of the tyrosine residue has a high energy penalty ($\Delta A_{ox}^{pt'} > 0$) in both catalases, albeit slightly larger for PVC ($\Delta\Delta A_{ox}^{pt'} = 0.10$ eV; see section 4.4). Adding up all contributions, we obtain estimates of $\Delta A = \Delta A_{red}^{pt} + \Delta A_{ox}^{pt'} = 0.08$ eV for HPC and 0.67 eV for PVC. Thus, radical migration is predicted to be close to thermoneutral in HPC, but it is clearly endergonic in PVC, in line with the experimental observation that radical migration occurs in HPC, but not in PVC. Moreover, the main determinant of this different behavior is that the free energy released by PT from the distal His to Fe=O in PVC is not large enough to compensate for the high energy penalty to be paid for the (PT-coupled) oxidation of Tyr318.

As noted above, our estimate for ΔA is based on two assumptions: (i) that the PT-coupled reduction free energy in HPC is the same as in HRP and (ii) that the oxidation free energy of the electron-donating Tyr residue and the pK_a values of the residue accepting the acidic proton of the tyrosine radical cation are the same as in aqueous solution. In the following we comment on the validity of these approximations. The heme reduction potential is known to be affected by the type of heme, the axial iron ligation, and the solvent accessibility.[69] Although both HPC and HRP contain the same type of heme (heme b), the negatively charged tyrosinate ligand in HPC is expected to increase ΔA_{red}^{pt} compared to the histidine ligand in HRP,[51a] whereas the buried heme pocket in HPC probably lowers ΔA_{red}^{pt} compared to the water-accessible active site in HRP. Altogether, we expect that the uncertainty in the absolute reduction potential of HPC is on the order of 0.1−0.2 eV. For instance, the $Fe^{3+}/^{2+}$

reduction potential of HRP[70] is 0.06 eV higher than that of BLC.[71] The uncertainty in the oxidation potential of tyrosine and the pK_a values of the protein residues is about 0.15 eV (see section 4.4). While these uncertainties may change the precise numerical value of ΔA within a reasonable range, they will not change our qualitative findings. That is, ΔA is near thermoneutral for HPC, but it is clearly positive for PVC. Thus, radical migration can occur spontaneously in HPC, but is thermodynamically unfavorable in PVC.

5. CONCLUDING REMARKS

In this work, we have investigated the main factors governing the formation of Cpd I* in two different catalases: HPC and PVC. The two proteins belong to different clades within the catalase family. HPC is a small subunit clade 3 catalase and contains heme b (iron protoporphyrin IX), similar to other catalases such as PMC, BLC, or HEC. Instead, PVC is a large subunit clade 2 catalase and contains heme d (Figure 1). Applying QM/MM molecular dynamics simulation, we have found that radical migration is more favored in HPC than in PVC ($\Delta\Delta A < 0$), supporting earlier suggestions that HPC forms a protein radical as opposed to PVC. We have also demonstrated that the different redox behaviors of the two proteins are due to the different energetics for PT from the distal histidine to the ferryl oxygen of reduced Cpd I. In HPC the free energy released by PT is large enough to compensate for the energy cost of removing an electron from the protein residue (tyrosine), as opposed to that of PVC. The lower basicity of the ferryl oxygen in PVC is probably related to the heme modification (heme d instead of heme b), which alters the nature of the electron-accepting orbital and with it the electron charge distribution that determines the proton affinity.

According to the reaction scheme in Figure 8, protein radical migration in HPC is "thermodynamically driven" by PT. This can be concluded irrespective of the mechanism of the PT-coupled radical migration, which we have not investigated in this work (PT followed by ET, ET followed by PT, or concerted). In other words, by stating that PT drives protein radical formation, we do not mean that PT occurs first and ET occurs second, but that ferryl oxygen protonation is required to make Cpd I* a stable species.

Our investigation confirms the view that heme b-containing catalases, such as HPC, are more prone to undergo radical migration than heme d-containing catalases, such as PVC. Our results also suggest that oxoferryl protonation is a key factor regulating radical migration in catalase and possibly also in other hydroperoxidases forming Cpd I*. Moreover, the present study points out the importance of hydrogen-bonding networks in the formation of tyrosyl radicals in catalases, similar to photosystem II[64] and the photosynthetic reaction centers.[59] The role of Tyr351 as a potential electron donor to the porphyrin radical cation of HPC may be probed by experimental EPR and mutagenesis studies of this residue.

■ ASSOCIATED CONTENT

Ⓢ Supporting Information. Setup of the classical molecular dynamics simulation (Figure S1), convergence of the calculations of the QM/MM energy gaps with respect to the QM size, cutoff radii, and sampling density (Figure S2 and Tables S1, S2, and S3, respectively), representative snapshots along the metadynamics trajectories of HPC and PVC (Figures S3 and S4, respectively), simulation parameters defining the metadynamics runs (Table S4), and complete ref 33. This material is available free of charge via the Internet at http://pubs.acs.org/.

■ AUTHOR INFORMATION

Corresponding Author
crovira@pcb.ub.es; j.blumberger@ucl.ac.uk

■ ACKNOWLEDGMENT

This work was supported by Grants SGR-2009-1309 from the Generalitat de Catalunya (GENCAT) and FIS2008-03845 from the Ministerio de Ciencia e Innovación (MICINN), Spain (to C.R.), a First Grant from the EPSRC (to H.O. and J.B.), and a University Research Fellowship and research grant from The Royal Society (to J.B.). The FI and BE fellowship programs of the GENCAT (to M.A.-P.) are also acknowledged. We further thank the Barcelona Supercomputing Center-Centro Nacional de Supercomputación (BSC-CNS) for the computer support, technical expertise, and assistance provided and the High Performance Computing Facility HECToR, Edinburgh, U.K., for computer time at the beginning of the project. We are also indebted to Prof. Ignacio Fita and Prof. Peter C. Loewen for very insightful discussions in the course of this work.

■ REFERENCES

(1) (a) Messerschmidt, A.; Huber, R.; Wieghardt, K.; Poulos, T. *Handbook of Metalloproteins*; Wiley: Chichester, U.K., 2001. (b) Zamocky, M.; Koller, F. *Prog. Biophys. Mol. Biol.* **1999**, *72*, 19–66.
(2) Halliwell, B.; Gutteridge, J. M. *Biochem. J.* **1984**, *219*, 1–14.
(3) Vuillaume, M. *Mutat. Res.* **1987**, *186*, 43–72.
(4) Yabuki, M.; Kariya, S.; Ishisaka, R.; Yasuda, T.; Yoshioka, T.; Horton, A. A.; Utsumi, K. *Free Radical Biol. Med.* **1999**, *26*, 325–332.
(5) Miyamoto, T.; Hayashi, M.; Takeuchi, A.; Okamoto, T.; Kawashima, S.; Takii, T.; Hayashi, H.; Onozaki, K. *J. Biochem.* **1996**, *120*, 725–730.
(6) (a) Alfonso-Prieto, M.; Borovik, A.; Carpena, X.; Murshudov, G.; Melik-Adamyan, W.; Fita, I.; Rovira, C.; Loewen, P. C. *J. Am. Chem. Soc.* **2007**, *129*, 4193–4205. (b) Rovira, C. *ChemPhysChem* **2005**, *6*, 1820–1826. (c) Horner, O.; Oddou, J. L.; Mouesca, J. M.; Jouve, H. M. *J. Inorg. Chem.* **2006**, *100*, 477–479. (d) Horner, O.; Mouesca, J. M.; Solari, P. L.; Orio, M.; Oddou, J. L.; Bonville, P.; Jouve, H. M. *J. Biol. Inorg. Chem.* **2007**, *12*, 509–525. (e) Green, M. T.; Dawson, J. H.; Gray, H. B. *Science* **2004**, *304*, 1653–1656.
(7) (a) Bonagura, C. A.; Bhaskar, B.; Shimizu, H.; Li, H.; Sundaramoorthy, M.; McRee, D. E.; Goodin, D. B.; Poulos, T. L. *Biochemistry* **2003**, *42*, 5600–5608. (b) Ivancich, A.; Jakopitsch, C.; Auer, M.; Un, S.; Obinger, C. *J. Am. Chem. Soc.* **2003**, *125*, 14093–14102.
(8) Fielding, A. J.; Singh, R.; Boscolo, B.; Loewen, P. C.; Ghibaudi, E. M.; Ivancich, A. *Biochemistry* **2008**, *47*, 9781–9792.
(9) (a) Ivancich, A.; Jouve, H. M.; Gaillard, J. *J. Am. Chem. Soc.* **1996**, *118*, 12852–12853. (b) Putnam, C. D.; Arvai, A. S.; Bourne, Y.; Tainer, J. A. *J. Mol. Biol.* **2000**, *296*, 295–309.
(10) Spolitak, T.; Dawson, J. H.; Ballou, D. P. *J. Inorg. Biochem.* **2006**, *100*, 2034–2044.
(11) (a) de Groot, H.; Auferkamp, O.; Bramey, T.; de Groot, K.; Kirsch, M.; Korth, H. G.; Petrat, F.; Sustmann, R. *Free Radical Res.* **2006**, *40*, 67–74. (b) Kirkman, H. N.; Gaetani, G. F. *Trends Biochem. Sci.* **2007**, *32*, 44–50.
(12) (a) Nichols, P.; Fita, I.; Loewen, P. C. In *Advanced Inorganic Chemistry*; Sykes, A. G., Mauk, G., Ed.; Academic Press: New York, 2001; pp 51−106. (b) Spolitak, T.; Dawson, J. H.; Ballou, D. P. *J. Biol. Inorg. Chem.* **2008**, *13*, 599–611.

(13) Smith, A. T.; Doyle, W. A.; Dorlet, P.; Ivancich, A. *Proc. Natl. Acad. Sci. U.S.A.* **2009**, *106*, 16084–16089.
(14) (a) Ivancich, A.; Jouve, H. M.; Sartor, B.; Gaillard, J. *Biochemistry* **1997**, *36*, 9356–9364. (b) Benecky, M. J.; Frew, J. E.; Scowen, N.; Jones, P.; Hoffman, B. M. *Biochemistry* **1993**, *32*, 11929–11933.
(15) (a) Blumberger, J.; Klein, M. L. *J. Am. Chem. Soc.* **2006**, *128*, 13854–13867. (b) Blumberger, J. *Phys. Chem. Chem. Phys.* **2008**, *10*, 5651–5667. (c) Tipmanee, V.; Oberhofer, H.; Park, M.; Kim, K. S.; Blumberger, J. *J. Am. Chem. Soc.* **2010**, *132*, 17032–17040.
(16) Laio, A.; Parrinello, M. *Proc. Natl. Acad. Sci. U.S.A.* **2002**, *99*, 12562–12566.
(17) Ensing, B.; De Vivo, M.; Liu, Z. W.; Moore, P.; Klein, M. L. *Acc. Chem. Res.* **2006**, *39*, 73–81.
(18) Leone, V.; Marinelli, F.; Carloni, P.; Parrinello, M. *Curr. Opin. Struct. Biol.* **2010**, *20*, 148–154.
(19) (a) Blumberger, J.; Ensing, B.; Klein, M. L. *Angew. Chem., Int. Ed.* **2006**, *45*, 2893–2897. (b) Blumberger, J.; Klein, M. L. *Chem. Phys. Lett.* **2006**, *422*, 210–217.
(20) Alfonso-Prieto, M.; Biarnes, X.; Vidossich, P.; Rovira, C. *J. Am. Chem. Soc.* **2009**, *131*, 11751–11761.
(21) Iannuzzi, M.; Laio, A.; Parrinello, M. *Phys. Rev. Lett.* **2003**, 90.
(22) Boero, M.; Ikeshoji, T.; Liew, C. C.; Terakura, K.; Parrinello, M. *J. Am. Chem. Soc.* **2004**, *126*, 6280–6286.
(23) (a) Roberts, J. E.; Hoffman, B. M.; Rutter, R.; Hager, L. P. *J. Biol. Chem.* **1981**, *256*, 2118–2121. (b) Kim, S. H.; Perera, R.; Hager, L. P.; Dawson, J. H.; Hoffman, B. M. *J. Am. Chem. Soc.* **2006**, *128*, 5598–5599. (c) Rittle, J.; Green, M. T. *Science* **2010**, *330*, 933–937.
(24) Schulz, C. E.; Rutter, R.; Sage, J. T.; Debrunner, P. G.; Hager, L. P. *Biochemistry* **1984**, *23*, 4743–4754.
(25) Theorell, H.; Ehrenberg, A. *Arch. Biochem. Biophys.* **1952**, *41*, 442–461.
(26) (a) Sivaraja, M.; Goodin, D. B.; Smith, M.; Hoffman, B. M. *Science* **1989**, *245*, 738–740. (b) Jakopitsch, C.; Obinger, C.; Un, S.; Ivancich, A. *J. Inorg. Biochem.* **2006**, *100*, 1091–1099. (c) Davydov, R.; Osborne, R. L.; Kim, S. H.; Dawson, J. H.; Hoffman, B. M. *Biochemistry* **2008**, *47*, 5147–5155.
(27) (a) Green, M. T. *J. Am. Chem. Soc.* **2001**, *123*, 9218–9219. (b) de Visser, S. P. *Inorg. Chem.* **2006**, *45*, 9551–9557. (c) Rovira, C.; Alfonso-Prieto, M.; Biarnés, X.; Carpena, X.; Fita, I.; Loewen, P. C. *Chem. Phys.* **2006**, *323*, 129–137.
(28) (a) Ghosh, A. *J. Am. Chem. Soc.* **1995**, *117*, 4691–4699. (b) Ghosh, A. *J. Phys. Chem. B* **1997**, *101*, 3290–3297. (c) Ghosh, A.; Vangberg, T. *Theor. Chem. Acc.* **1997**, *97*, 143–149.
(29) Liao, M. S.; Scheiner, S. *J. Chem. Phys.* **2002**, *117*, 205–219.
(30) The implementation of the BP86 functional in Dmol and ADF (used in the Ghosh[28] and Scheiner[29] studies, respectively) is slightly different from that in the CPMD program used in this work. Specifically, in Dmol and ADF the Vosko−Wilk−Nusair (VWN) parametrization of the correlation energy of the homogeneous electron gas is used, whereas CPMD uses the Perdew−Zunger fit.
(31) Zhao, Y.; Truhlar, D. G. *J. Chem. Phys.* **2006**, *125*, 194101–194118.
(32) Derat, E.; Shaik, S. *J. Am. Chem. Soc.* **2006**, *128*, 8185–8198.
(33) Frisch, M. J.; et al. *GAUSSIAN 03*; Gaussian Inc.: Wallingford, CT, 2004.
(34) Junmei, W.; Wei, W.; Kollman, P. A.; Case, D. A. *J. Mol. Graphics Modell.* **2006**, *25*, 247–260.
(35) Pearlman, D. A.; Case, D. A.; Caldwell, J. W.; Ross, W. S.; Cheatham, T. E.; Debolt, S.; Ferguson, D.; Seibel, G.; Kollman, P. *Comput. Phys. Commun.* **1995**, *91*, 1–41.
(36) Humphrey, W.; Dalke, A.; Schulten, K. *J. Mol. Graphics* **1996**, *14*, 33.
(37) Car, R.; Parrinello, M. *Phys. Rev. Lett.* **1985**, *55*, 2471–2474.
(38) (a) Becke, A. D. *Phys. Rev. A* **1988**, *38*, 3098–3100. (b) Perdew, J. P. *Phys. Rev. B* **1986**, *33*, 8822–8824.
(39) (a) Alfonso-Prieto, M.; Vidossich, P.; Rodriguez-Fortea, A.; Carpena, X.; Fita, I.; Loewen, P. C.; Rovira, C. *J. Phys. Chem. A* **2008**, *112*, 12842–12848. (b) Vidossich, P.; Alfonso-Prieto, M.; Carpena, X.; Loewen, P. C.; Fita, I.; Rovira, C. *J. Am. Chem. Soc.* **2007**, *129*, 13436–13446. (c) Rovira, C.; Kunc, K.; Hutter, J.; Ballone, P.; Parrinello, M. *J. Phys. Chem. A* **1997**, *101*, 8914–8925.
(40) Laio, A.; VandeVondele, J.; Rothlisberger, U. *J. Chem. Phys.* **2002**, *116*, 6941–6947.
(41) Laio, A.; VandeVondele, J.; Rothlisberger, U. *J. Phys. Chem. B* **2002**, *106*, 7300–7307.
(42) Hunenberger, P. H. *J. Chem. Phys.* **2000**, *113*, 10464–10476.
(43) Timkovich, R.; Bondoc, L. L. *Advances in Biophysical Chemistry*; JAI Press: Greenwich, CT, 1990; Vol. 1.
(44) (a) Hanson, L. K.; Chang, C. K.; Davis, M. S.; Fajer, J. *J. Am. Chem. Soc.* **1981**, *103*, 663–670. (b) Ozawa, S.; Fujii, H.; Morishima, I. *J. Am. Chem. Soc.* **1992**, *114*, 1548–1554. (c) Ozawa, S.; Watanabe, Y.; Morishima, I. *Inorg. Chem.* **1992**, *31*, 4042–4043. (d) Ozawa, S.; Watanabe, Y.; Morishima, I. *J. Am. Chem. Soc.* **1994**, *116*, 5832–5838. (e) Jayaraj, K.; Gold, A.; Austin, R. N.; Mandon, D.; Weiss, R.; Terner, J.; Bill, E.; Muther, M.; Trautwein, A. X. *J. Am. Chem. Soc.* **1995**, *117*, 9079–9080.
(45) Note that although the location of the TS is at CV1 = 0, CV2 = −0.2 for both enzymes, the corresponding TS structures differ because different parameters were used to define CV1 and CV2 for the two enzymes.
(46) The pK_a of the distal His in BLC and HRP is based on the pH-dependent shift of the Fe=O stretching frequency in resonance Raman (RR) experiments. The shift is attributed to deprotonation of the distal His, which changes the hydrogen bond pattern connecting the distal His and the oxoferryl unit. Nevertheless, the difficulty in characterizing the Fe−OH band in RR experiments (see the discussion in ref 48) precludes considering a scenario in which the extra proton is shared between the distal His and the oxoferryl, and thus, the pK_a of the distal His is likely to be overestimated.
(47) Jones, P.; Dunford, H. B. *J. Inorg. Biochem.* **2005**, *99*, 2292–2298.
(48) Silaghi-Dumitrescu, R.; Reeder, B. J.; Nicholls, P.; Cooper, C. E.; Wilson, M. T. *Biochem. J.* **2007**, *403*, 391–395.
(49) Behan, R. K.; Green, M. T. *J. Inorg. Biochem.* **2006**, *100*, 448–459.
(50) Green, M. T. *J. Am. Chem. Soc.* **2006**, *128*, 1902–1906.
(51) (a) Rydberg, P.; Sigfridsson, E.; Ryde, U. *J. Biol. Inorg. Chem.* **2004**, *9*, 203–223. (b) Wang, R.; de Visser, S. P. *J. Inorg. Biochem.* **2007**, *101*, 1464–1472.
(52) Svistunenko, D. A. *Biochim. Biophys. Acta* **2005**, *1707*, 127–155.
(53) (a) Moser, C. C.; Page, C. C.; Dutton, P. L. *Philos. Trans. R. Soc. London, B* **2006**, *361*, 1295–1305. (b) Reece, S. Y.; Hodgkiss, J. M.; Stubbe, J.; Nocera, D. G. *Philos. Trans. R. Soc. London, B* **2006**, *361*, 1351–1364.
(54) (a) Onuchic, J. N.; Beratan, D. N.; Winkler, J. R.; Gray, H. B. *Annu. Rev. Biophys. Biomol. Struct.* **1992**, *21*, 349–377. (b) Gray, H. B.; Winkler, J. R. *Annu. Rev. Biochem.* **1996**, *65*, 537–561.
(55) Guallar, V. *J. Phys. Chem. B* **2008**, *112*, 13460–13464.
(56) Guallar, V.; Wallrapp, F. *J. R. Soc. Interface* **2008**, *5* (Suppl 3), S233–239.
(57) Dixon, W. T.; Murphy, D. *J. Chem. Soc., Faraday Trans. 2* **1976**, *72*, 1221–1230.
(58) Beratan, D. N.; Onuchic, J. N.; Winkler, J. R.; Gray, H. B. *Science* **1992**, *258*, 1740–1741.
(59) Narvaez, A. J.; LoBrutto, R.; Allen, J. P.; Williams, J. C. *Biochemistry* **2004**, *43*, 14379–14384.
(60) Sjödin, M.; Irebo, T.; Utas, J. E.; Lind, J.; Merenyi, G.; Akermark, B.; Hammarstrom, L. *J. Am. Chem. Soc.* **2006**, *128*, 13076–13083.
(61) (a) Henry, B.; Tekely, P.; Delpuech, J. J. *J. Am. Chem. Soc.* **2002**, *124*, 2025–2034. (b) Nozaki, Y.; Tanford, C. *J. Biol. Chem.* **1967**, *242*, 4731–4735.
(62) Hay, S.; Westerlund, K.; Tommos, C. *Biochemistry* **2005**, *44*, 11891–11902.
(63) (a) O'Malley, P. J. *J. Am. Chem. Soc.* **1998**, *120*, 11732–11737. (b) Blomberg, M. R. A.; Siegbahn, P. E. M.; Babcock, G. T. *J. Am. Chem. Soc.* **1998**, *120*, 8812–8824. (c) Wang, Y. N.; Eriksson, L. A. *Int. J.*

Quantum Chem. **2001**, *83*, 220–229. (d) Zhang, Y.; Huang, K. X. *J. Mol. Struct.: THEOCHEM* **2008**, *864*, 48–55.
(64) Hays, A. M.; Vassiliev, I. R.; Golbeck, J. H.; Debus, R. J. *Biochemistry* **1999**, *38*, 11851–11865.
(65) Maximum pK_a difference for glutamate residues hydrogen-bonded to arginine (E13, E20) in the AB leucine zipper reported in ref 67a.
(66) Average pK_a difference for glutamate residues with two hydrogen bonds reported in ref 67b.
(67) (a) Gorfe, A. A.; Ferrara, P.; Caflisch, A.; Marti, D. N.; Bosshard, H. R.; Jelesarov, I. *Proteins: Struct., Funct., Genet.* **2002**, *46*, 41–60. (b) Forsyth, W. R.; Antosiewiez, J. M.; Robertson, A. D. *Proteins: Struct., Funct., Genet.* **2002**, *48*, 388–403.
(68) Hayashi, Y.; Yamazaki, I. *J. Biol. Chem.* **1979**, *254*, 9101–9106.
(69) (a) Battistuzzi, G.; Borsari, M.; Cowan, J. A.; Ranieri, A.; Sola, M. *J. Am. Chem. Soc.* **2002**, *124*, 5315–5324. (b) Tezcan, F. A.; Winkler, J. R.; Gray, H. B. *J. Am. Chem. Soc.* **1998**, *120*, 13383–13388.
(70) Tanaka, M.; Nagano, S.; Ishimori, K.; Morishima, I. *Biochemistry* **1997**, *36*, 9791–9798.
(71) Reedy, C. J.; Elvekrog, M. M.; Gibney, B. R. *Nucleic Acids Res.* **2008**, *36*, D307–313.
(72) Andreoletti, P.; Sainz, G.; Jaquinod, M.; Gagnon, J.; Jouve, H. M. *Proteins* **2003**, *50*, 261–271.
(73) (a) Nilsson, K.; Ryde, U. *J. Inorg. Biochem.* **2004**, *98*, 1539–1546. (b) Sicking, W.; Korth, H. G.; de Groot, H.; Sustmann, R. *J. Am. Chem. Soc.* **2008**, *130*, 7345–7356.
(74) Berglund, G. I.; Carlsson, G. H.; Smith, A. T.; Szoke, H.; Henriksen, A.; Hajdu, J. *Nature* **2002**, *417*, 463–468.
(75) (a) Bathelt, C. M.; Mulholland, A. J.; Harvey, J. N. *Dalton Trans.* **2005**, 3470–3476. (b) Derat, E.; Cohen, S.; Shaik, S.; Altun, A.; Thiel, W. *J. Am. Chem. Soc.* **2005**, *127*, 13611–13621.
(76) Deeth, R. J. *J. Am. Chem. Soc.* **1999**, *121*, 6074–6075.
(77) (a) Silaghi-Dumitrescu, R. *J. Biol. Inorg. Chem.* **2004**, *9*, 471–476. (b) Silaghi-Dumitrescu, R.; Cooper, C. E. *Dalton Trans.* **2005**, 3477–3482.
(78) Stone, K. L.; Behan, R. K.; Green, M. T. *Proc. Natl. Acad. Sci. U.S.A.* **2005**, *102*, 16563–16565.
(79) Schlichting, I.; Berendzen, J.; Chu, K.; Stock, A. M.; Maves, S. A.; Benson, D. E.; Sweet, R. M.; Ringe, D.; Petsko, G. A.; Sligar, S. G. *Science* **2000**, *287*, 1615–1622.
(80) (a) Hersleth, H. P.; Ryde, U.; Rydberg, P.; Gorbitz, C. H.; Andersson, K. K. *J. Inorg. Biochem.* **2006**, *100*, 460–476. (b) Stone, K. L.; Hoffart, L. M.; Behan, R. K.; Krebs, C.; Green, M. T. *J. Am. Chem. Soc.* **2006**, *128*, 6147–6153. (c) Schoneboom, J. C.; Lin, H.; Reuter, N.; Thiel, W.; Cohen, S.; Ogliaro, F.; Shaik, S. *J. Am. Chem. Soc.* **2002**, *124*, 8142–8151. (d) Ogliaro, F.; Cohen, S.; Filatov, M.; Harris, N.; Shaik, S. *Angew. Chem., Int. Ed.* **2001**, *40*, 647. (e) Harris, N.; Cohen, S.; Filatov, M.; Ogliaro, F.; Shaik, S. *Angew. Chem., Int. Ed.* **2000**, *39*, 2003–2007.
(81) Murshudov, G. N.; Grebenko, A. I.; Brannigan, J. A.; Antson, A. A.; Barynin, V. V.; Dodson, G. G.; Dauter, Z.; Wilson, K. S.; Melik-Adamyan, W. R. *Acta Crystallogr., D: Biol. Crystallogr.* **2002**, *58*, 1972–1982.
(82) Ghosh, A. *J. Biol. Inorg. Chem.* **2006**, *11*, 712–724.
(83) (a) Wasinger, E. C.; de Groot, F. M.; Hedman, B.; Hodgson, K. O.; Solomon, E. I. *J. Am. Chem. Soc.* **2003**, *125*, 12894–12906. (b) Daiber, A.; Herold, S.; Schoneich, C.; Namgaladze, D.; Peterson, J. A.; Ullrich, V. *Eur. J. Biochem.* **2000**, *267*, 6729–6739.
(84) Chance, M.; Powers, L.; Kumar, C.; Chance, B. *Biochemistry* **1986**, *25*, 1259–1265.
(85) Jakopitsch, C.; Auer, M.; Ivancich, A.; Ruker, F.; Furtmuller, P. G.; Obinger, C. *J. Biol. Chem.* **2003**, *278*, 20185–20191.
(86) Ghosh, A.; Almlof, J.; Que, L. *J. Phys. Chem.* **1994**, *98*, 5576–5579.
(87) Harris, D.; Loew, G. *J. Am. Chem. Soc.* **1995**, *117*, 2738–2746.
(88) Kuramochi, H.; Noodleman, L.; Case, D. A. *J. Am. Chem. Soc.* **1997**, *119*, 11442–11451.
(89) Newcomb, M.; Halgrimson, J. A.; Horner, J. H.; Wasinger, E. C.; Chen, L. X.; Sligar, S. G. *Proc. Natl. Acad. Sci. U.S.A.* **2008**, *105*, 8179–8184.
(90) (a) Behan, R. K.; Hoffart, L. M.; Stone, K. L.; Krebs, C.; Green, M. T. *J. Am. Chem. Soc.* **2006**, *128*, 11471–11474. (b) Stone, K. L.; Behan, R. K.; Green, M. T. *Proc. Natl. Acad. Sci. U.S.A.* **2006**, *103*, 12307–12310. (c) Lai, W.; Chen, H.; Shaik, S. *J. Phys. Chem. B* **2009**, *113*, 7912–7917.
(91) Filatov, M.; Harris, N.; Shaik, S. *J. Chem. Soc., Perkin Trans.* **1999**, *2*, 399–410.
(92) Harris, D. L.; Loew, G. H. *J. Am. Chem. Soc.* **1998**, *120*, 8941–8948.
(93) Altun, A.; Kumar, D.; Neese, F.; Thiel, W. *J. Phys. Chem. A* **2008**, *112*, 12904–12910.
(94) Chen, H.; Song, J. S.; Lai, W. Z.; Wu, W.; Shaik, S. *J. Chem. Theor. Comput.* **2010**, *6*, 940–953.
(95) Chen, H.; Hirao, H.; Derat, E.; Schlichting, I.; Shaik, S. *J. Phys. Chem. B* **2008**, *112*, 9490–9500.
(96) (a) Margoliash, E.; Novogrodsky, A.; Schejter, A. *Biochem. J.* **1960**, *74*, 339–348. (b) Kikuchi, K.; Kawamura-Konishi, Y.; Suzuki, H. *Arch. Biochem. Biophys.* **1992**, *296*, 88–94.
(97) Chuang, W. J.; Heldt, J.; Van Wart, H. E. *J. Biol. Chem.* **1989**, *264*, 14209–14215.
(98) (a) Obinger, C.; Maj, M.; Nicholls, P.; Loewen, P. *Arch. Biochem. Biophys.* **1997**, *342*, 58–67. (b) Chelikani, P.; Carpena, X.; Perez-Luque, R.; Donald, L. J.; Duckworth, H. W.; Switala, J.; Fita, I.; Loewen, P. C. *Biochemistry* **2005**, *44*, 5597–5605.